

Metropolis Monte Carlo and Wang-Landau Simulations of Tricriticality in Crossed Ising Chains

T. Cary, R.R.P. Singh and R.T. Scalettar

Department of Physics, One Shields Ave., University of California, Davis, California 95616, USA

We explore the phase diagram of Ising spins on one-dimensional chains which criss-cross in two perpendicular directions and are connected by interchain couplings. This system is of interest as a simpler, classical analog of a quantum Hamiltonian which has been proposed as a model of magnetic behavior in $\text{Nb}_{12}\text{O}_{29}$ and also, conceptually, as a geometry which is intermediate between one and two dimensions. Using mean field theory as well as Metropolis Monte Carlo and Wang-Landau simulations, we locate quantitatively the boundaries of four ordered phases. Each becomes an effective Ising model with unique effective couplings at large interchain coupling. Away from this limit we demonstrate non-trivial critical behavior, including tricritical points which separate first and second order phase transitions. Finally, we find that the crossover of the magnetization critical exponent from the Ising to tricritical Ising value shows an unusual non-monotonic behavior.

PACS numbers: 71.10.Fd, 71.30.+h, 02.70.Uu

INTRODUCTION

Dimensionality, along with order parameter symmetry, plays a decisive role in the occurrence of phase transitions and the critical exponents with which they are characterized[1]. Beginning with simple, regular geometries, critical properties are now well-understood in more complex geometries in which the dimensionality is more ambiguous, including diluted lattices[2], fractal geometries[3], and networks with longer range interactions[4–8].

Recently there has been interest in a further class of systems of “mixed geometry” whose underlying structure consists of two perpendicular collections of one dimensional chains which are then further connected to form a two dimensional framework. For example, it has been suggested[9] that an appropriate model of magnetic phase transitions in one of the niobates, $\text{Nb}_{12}\text{O}_{29}$, consists of one dimensional chains of localized (Heisenberg) spins and a further perpendicularly oriented set of one dimensional conduction electron chains. These two types of spins reflect the presence of distinct Nb cations with $4d^1$ configuration, one of which exhibits local moment behavior and the other being itinerant and Pauli paramagnetic[10, 11]. In this model, the electron spins on the conducting nanowires are coupled to the Heisenberg chains by a Kondo interaction on each site.

Similarly, in optical lattices[12], bosonic or fermionic atoms can occupy higher, spatially anisotropic, p_x and p_y orbitals which allow hopping which is essentially just along one-dimensional chains. Within a given well, atoms can convert from occupying the p_x to occupying the p_y orbital, thus coupling the perpendicular chains and providing a two dimensional character to the system. Bosonic systems in this geometry can exhibit exotic forms of superfluidity whose condensate wave functions belong to non-trivial representations of the lattice point group, with condensation accompanied by

unusual columnar, antiferromagnetic, and Mott phases [13–16]. Models in which fermionic degrees of freedom in the two orbitals have Hund’s rule type coupling have also been considered, and shown rigorously to exhibit magnetic order[17].

These examples share a common “1D \times 1D” geometrical structure in which one type of chain has degrees of freedom which are coupled in the \hat{x} direction, while the degrees of freedom of the other couple in the \hat{y} direction. An additional interaction on each lattice site connects the two sets of chains. Although considerable progress has been made in modeling the niobates and p-wave bosons in optical lattices, in both cases the quantum nature of the spins makes achieving a definitive understanding of the critical phenomena quite challenging. The goal of this paper is to examine a classical Ising model on this type of lattice. We will show that the interchain coupling is sufficient to promote long range order at finite temperature, and that the phase transitions can exhibit a rich variety of behaviors including tricritical points.

MODEL AND METHODS

We consider the following model,

$$\begin{aligned}
 E = & -J_x \sum_{\mathbf{r}} S_{\mathbf{r}} S_{\mathbf{r}+\hat{x}} - J_y \sum_{\mathbf{r}} T_{\mathbf{r}} T_{\mathbf{r}+\hat{y}} \\
 & -J_K \sum_{\mathbf{r}} S_{\mathbf{r}} T_{\mathbf{r}} - J_{K'} \sum_{\mathbf{r}} S_{\mathbf{r}} (T_{\mathbf{r}+\hat{y}} + T_{\mathbf{r}-\hat{y}}) \\
 & -J_{K'} \sum_{\mathbf{r}} T_{\mathbf{r}} (S_{\mathbf{r}+\hat{x}} + S_{\mathbf{r}-\hat{x}})
 \end{aligned} \tag{1}$$

which we will refer to as the crossed Ising chains model (CICM).

Here $S_{\mathbf{r}}$ and $T_{\mathbf{r}}$ are Ising spins (i.e. they can have a value of either +1 or -1) coupled into one-dimensional

chains in the \hat{x} and \hat{y} directions, respectively. These spins occupy a two-dimensional, square, $L \times L$ lattice with periodic boundary conditions. There is an S and a T spin on each of the $N=L^2$ sites and therefore, $2N$ total spins in the system. J_K and $J_{K'}$ couple S and T spins on the same lattice site and near neighbor sites, respectively. The geometry of Eq. 1 is illustrated in Fig. 1. For simplicity, and also because this choice is the appropriate one for several of the physical realizations of the CICM, we will set $J_x = J_y = J_{x,y} = 1$ and measure all energies in units of $J_{x,y}$.

Initial insight into the phase diagram of this model is obtained by considering $T = 0$ and minimizing the internal energy, Eq. 1. Fig. 2 shows the definitions of the four ordered phases which can occur: ferromagnetic (FM), ferromagnetic-prime (FM'), antiferromagnetic (AFM), and antiferromagnetic-prime (AFM'). The phase diagram at $T = 0$ is shown in Fig. 3. The CICM has the symmetry that changing the signs of J_K and $J_{K'}$ changes the phase from FM to AFM or AFM to FM and FM' to AFM' or AFM' to FM'. If J_K and $J_{K'}$ are both positive or both negative, there will be no competition between ordered phases and the model will have relatively uninteresting features, namely a conventional second order phase transition between a high temperature disordered paramagnetic (PM) phase and a low temperature FM phase or AFM phase, respectively. However, if only one of the interchain couplings is negative, there will be a competition between ordered phases and the most interesting physics will result.

The total spin, $S_{\mathbf{r}} + T_{\mathbf{r}}$, on a site can take on the three values, $-2, 0$, or $+2$, giving the CICM some similarity to the two-dimensional square lattice Blume-Capel model [18, 19],

$$E = -J \sum_{\langle ij \rangle} M_i M_j + \Delta \sum_i M_i^2 \quad (2)$$

which is a spin 1 generalization of the Ising model where $M_i = -1, 0$, or $+1$. The choice $J_K < 0$ favors $S_{\mathbf{r}} = -T_{\mathbf{r}}$ and hence $S_{\mathbf{r}} + T_{\mathbf{r}} = 0$ so that the strength of J_K plays a role similar to that of the vacancy potential Δ whose energy ΔM_i^2 can tune the density of sites with $M_i = 0$.

The remainder of this paper is organized as follows. We begin our discussion of Eq. 1 via a mean field treatment. The resulting phase diagrams, as in the case of the BCM, will be shown to correctly predict certain qualitative features of the CICM such as the presence of ordered phases, effective Ising regimes in the large $|J_K|$ limit, and tricritical points. We then turn to an exact Monte Carlo (MC) approach which allows a more accurate quantitative determination of the phase diagram. We use the standard single spin-flip Metropolis MC algorithm, supplemented by some cluster flips. The data are analyzed with standard numerical approaches, including

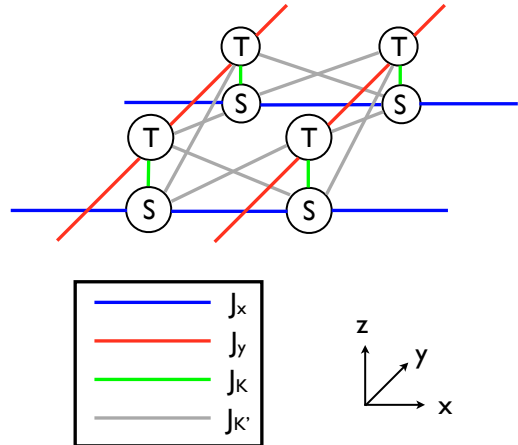


FIG. 1: (Color online) The geometry of the interactions in the CICM for four sites is shown. This model is studied on an $L \times L$ square lattice with periodic boundary conditions (in the \hat{x} and \hat{y} directions) containing $N (= L^2)$ “S spins” and N “T spins” taking values ± 1 . There are L parallel 1D chains of S spins in the \hat{x} direction and L parallel 1D chains of T spins in the \hat{y} direction, illustrated by the blue (J_x) and red (J_y) lines, respectively. There is an interaction between an S and a T spin on the same site in the \hat{z} direction (J_K) illustrated by the green lines. Finally, there is an interaction between nearest neighbor S and T spins ($J_{K'}$) which is illustrated by the gray lines.

the use of the Binder fourth order cumulant [20]. The results show that there are four ordered phases, each of which becomes an effective Ising model in the large $|J_K|$ limit with unique effective couplings. Additionally, the presence of tricritical points is confirmed. In order to provide further corroboration for the nature of the phase transitions, we also employ the Wang-Landau algorithm [21–23] to obtain the density of states and the behavior of canonical distributions as a function of temperature when passing through first and second order phase transitions. We find that this algorithm is particularly well suited for verifying the order of a phase transition and therefore the existence of tricritical points. Finally, we find that the crossover of critical exponent values from Ising to tricritical Ising shows an unusual non-monotonic behavior. As one approaches the tricritical point, the magnetization exponent 2β obtained from log-log plots of the magnetization squared with reduced temperature, at the length scale of our simulations, at first rises well above the well known Ising value of $2\beta = \frac{1}{4}$ to approximately 0.41 before falling sharply to approximately 0.13, close to the expected tricritical Ising value of $2\beta = \frac{1}{12}$. A similar non-monotonic behavior is also observed in simulations of the Blume-Capel model.

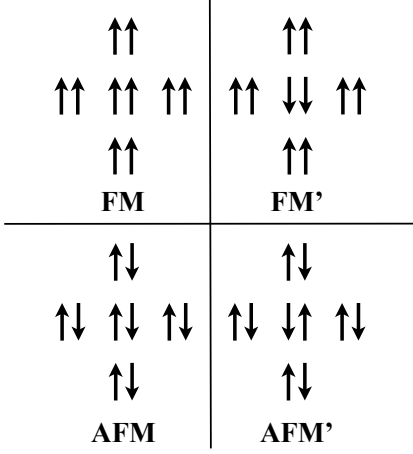


FIG. 2: The four ordered phases found in the CICM are defined. Each pair of spins represents an S and a T spin on a single site (i.e. coupled by J_K). In the ferromagnetic (FM) phase, all S and T spins are aligned ferromagnetically. In the ferromagnetic prime (FM') phase, the S and T spins are aligned ferromagnetically on each site and antiferromagnetically along the S and T chains. In the antiferromagnetic (AFM) phase, the S and T spins are aligned antiferromagnetically on each site and ferromagnetically along the S and T chains. Finally, in the antiferromagnetic-prime (AFM') phase, the S and T spins are aligned antiferromagnetically on each site and also along the S and T chains. There is spin inversion symmetry in this model so flipping all of the spins in any of these phases does not change the phase.

MEAN FIELD THEORY

We solve Eq. 1 by replacing the two spin interactions with a single spin coupled to a self-consistently determined average spin value

$$m_1 \equiv \langle S_r \rangle \quad m_2 \equiv \langle T_r \rangle. \quad (3)$$

In the case of the FM' and AFM' phases, these order parameters alternate in sign on the (bipartite) lattice.

The resulting implicit equations for the order parameters, $m_{FM}=m_1=m_2$ and $m_{AFM}=m_1=-m_2$ ($\beta = \frac{1}{T}$ and $k_B = 1$),

$$\begin{aligned} m_{FM} &= \frac{\sinh(4\beta m_{FM}(J_{x,y} + 2J_{K'}))}{\cosh(4\beta m_{FM}(J_{x,y} + 2J_{K'})) + e^{-2\beta J_K}} \\ m_{AFM} &= \frac{\sinh(4\beta m_{AFM}(J_{x,y} - 2J_{K'}))}{\cosh(4\beta m_{AFM}(J_{x,y} - 2J_{K'})) + e^{2\beta J_K}} \end{aligned} \quad (4)$$

are solved using Newton's method. Equivalently, the mean field free energy of the CICM can be expanded in a power series in the order parameter for both the FM and AFM phases and the critical temperature for a second order phase transition determined by calculating the temperature where the coefficient of the quadratic

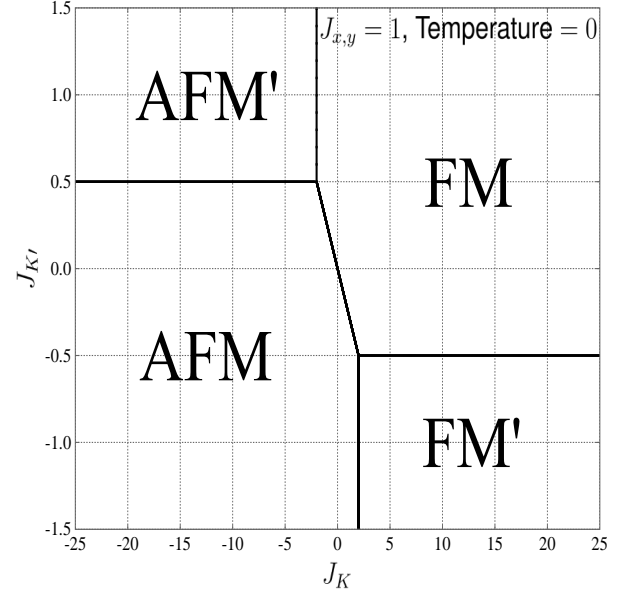


FIG. 3: The phase diagram for the CICM with $J_{x,y}=1$ and $T=0$ in the $J_{K'}$ versus J_K parameter space is shown. The line separating the FM and AFM phases (where the internal energies are equal) is given by $J_{K'} = -\frac{1}{4}J_K$. The AFM and AFM' phases are separated by $J_{K'} = \frac{J_{x,y}}{2} = \frac{1}{2}$; the FM and FM' phases by $J_{K'} = \frac{-J_{x,y}}{2} = -\frac{1}{2}$; the FM and AFM' phases by $J_K = -2J_{x,y} = -2$; and the AFM and FM' phases by $J_K = 2J_{x,y} = 2$. This phase diagram is consistent with the observation that for J_K and $J_{K'}$ both positive or both negative, there is no competition between phases. Additionally, the symmetry between FM and AFM and FM' and AFM' when switching the signs of J_K and $J_{K'}$ is evident.

term in the free energy expansion vanishes. The implicit equations for the FM and AFM second order critical lines are,

$$\begin{aligned} T_{C,FM} &= \frac{4(J_{x,y} + 2J_{K'})}{1 + e^{\frac{-2J_K}{T_{C,FM}}}} \\ T_{C,AFM} &= \frac{4(J_{x,y} - 2J_{K'})}{1 + e^{\frac{2J_K}{T_{C,AFM}}}}. \end{aligned} \quad (5)$$

Tricritical points are located by calculating the temperature at which the quartic coefficient in the expansion of the free energy vanishes,

$$\begin{aligned} T_{\text{tricritical, FM}} &= \frac{-2}{\ln(2)} J_K \\ T_{\text{tricritical, AFM}} &= \frac{2}{\ln(2)} J_K. \end{aligned} \quad (6)$$

Combining this with the condition for intersecting the second order phase boundary, simple analytic expressions for the coordinates of the mean field tricritical points can be written down.

$$\begin{aligned}
T_{\text{tricritical point, FM}} &= \frac{4(J_{x,y} + 2J_{K'})}{3} \\
J_{K,\text{tricritical point, FM}} &= \frac{-2\ln(2)(J_{x,y} + 2J_{K'})}{3} \\
T_{\text{tricritical point, AFM}} &= \frac{4(J_{x,y} - 2J_{K'})}{3} \\
J_{K,\text{tricritical point, AFM}} &= \frac{2\ln(2)(J_{x,y} - 2J_{K'})}{3} \quad (7)
\end{aligned}$$

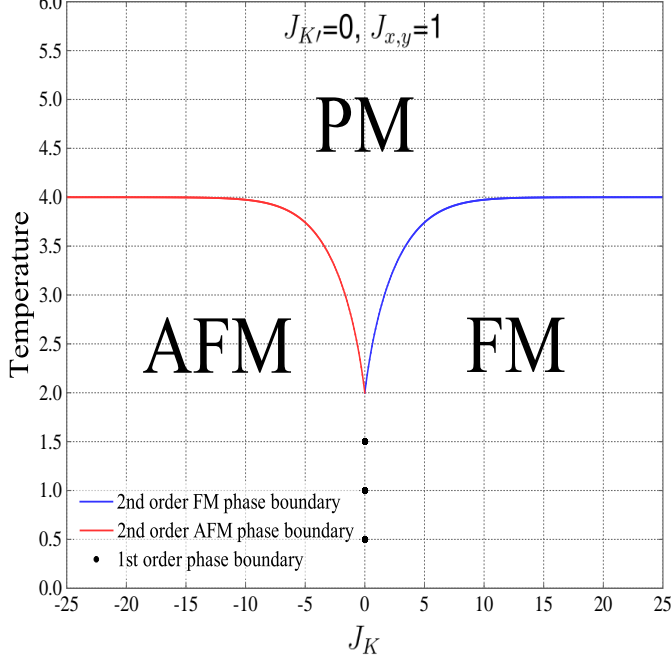


FIG. 4: (Color online) The mean field theory phase diagram for $J_{K'} = 0$ and $J_{x,y} = 1$ is shown. For these parameters, there is no tricritical point. For $J_K > 0$, there is a second order phase transition between a low temperature FM phase and a high temperature PM phase. For $J_K < 0$, there is a second order phase transition between a low temperature AFM phase and a high temperature PM phase. Also, there is a vertical first order phase boundary between the FM and AFM phases at $J_K = 0$ which extends up to $T = 2$, the MF critical temperature. In the large, positive J_K limit, this model becomes an effective 2D Ising model with $T_C = 4(J_{x,y} + 2J_{K'}) = 4$. In the large, negative J_K limit, this model also becomes an effective 2D Ising model with $T_C = 4(J_{x,y} - 2J_{K'}) = 4$. The FM and AFM phase shapes are symmetric about $J_K = 0$ only when $J_{K'} = 0$.

To find the first order phase boundary once the tricritical point has been reached, simultaneous plots of the FM and AFM free energy were made and temperature or J_K was incremented to find the point where the phase with the global minimum changes.

For $J_{K'} = 0$, the mean field phase diagram (Fig. 4) shows no tricritical point, making it clear that $J_{K'}$ is crucial for the onset of first order phase transitions.

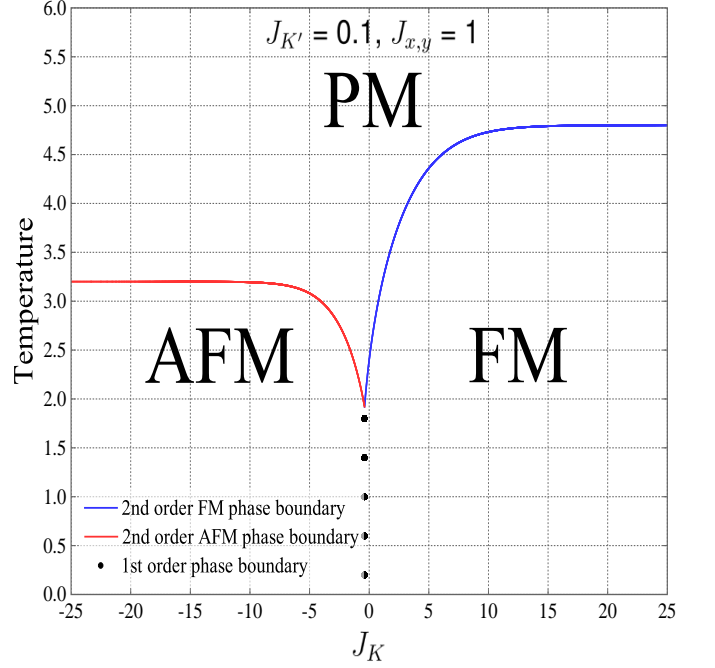


FIG. 5: (Color online) The mean field theory phase diagram for $J_{K'} = 0.1$ and $J_{x,y} = 1$ is shown. For these parameters, there is no tricritical point. For $J_K > -4J_{K'} = -0.4$, there is a second order phase transition between a low temperature FM phase and a high temperature PM phase. For $J_K < -4J_{K'} = -0.4$, there is a second order phase transition between a low temperature AFM phase and a high temperature PM phase. Also, there is a vertical first order phase boundary between the FM and AFM phases at $J_K = -0.4$. In the large, positive J_K limit, this model becomes an effective 2D Ising model with $T_C = 4(J_{x,y} + 2J_{K'}) = 4.8$. In the large, negative J_K limit, this model also becomes an effective 2D Ising model with $T_C = 4(J_{x,y} - 2J_{K'}) = 3.2$. A positive $J_{K'}$ shrinks the AFM phase and grows the FM phase as it is increased in magnitude, as evidenced by comparing with the phase diagram for $J_{K'} = 0$.

The AFM phase arises for $J_K < 0$, as expected, since negative J_K antiferromagnetically couples the S and T spins on shared sites. For $J_K > 0$, the FM phase arises. The mean field phase boundary separating the FM and AFM phases at $T = 0$ where thermal fluctuations are nonexistent agrees with the ground state phase diagram in Fig. 3. The MFT critical temperature $T_C = 2$ at $J_K = 0$ and $J_{K'} = 0$, as expected since the CICM decouples into independent 1D Ising chains. For large $|J_K|$, the S and T spin pairs on each site lose their independence due to the high energy cost of flipping only one of the spins in a pair. In this limit, the model becomes an effective 2D Ising model with $J_{\text{eff,FM}} = J_{x,y} + 2J_{K'}$ and $J_{\text{eff,AFM}} = J_{x,y} - 2J_{K'}$ for positive and negative J_K , respectively. This leads to the limiting values $T_C = 4$ for $|J_K|$ large in Fig. 4.

In fact, this single “locked spin” Ising regime in the large $|J_K|$ limit occurs for all four ordered phases.

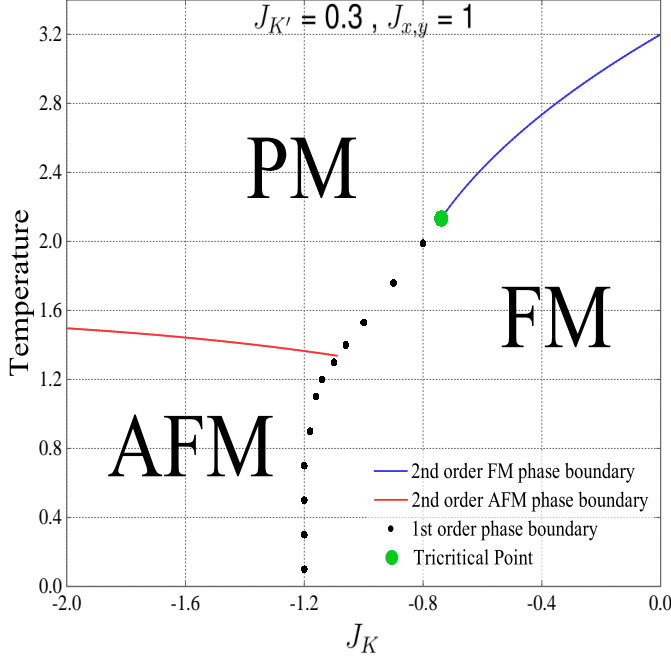


FIG. 6: (Color online) The mean field theory phase diagram for $J_{K'} = 0.3$ and $J_{x,y} = 1$ is shown. For $J_K \gtrsim -0.7$, there is a second order phase transition between a low temperature FM phase and a high temperature PM phase. For $-1.1 \lesssim J_K \lesssim -0.7$, there is a first order phase transition between a low temperature FM phase and a high temperature PM phase. This section of the phase diagram is separated from the previous section by the green tricritical point (located at $T = \frac{32}{15} \approx 2.13$, $J_K = \frac{-16 \ln(2)}{15} \approx -0.74$). For $-1.2 \lesssim J_K \lesssim -1.1$ there is a low temperature FM phase followed by a small higher temperature AFM phase and then, for higher temperatures, a disordered PM phase. For $J_K \lesssim -1.2$ there is a second order phase boundary between a low temperature AFM phase and a high temperature PM phase. Additionally, there is an approximately vertical first order phase boundary between the FM and AFM phases at $J_K = -1.2$. This phase diagram is zoomed in relative to the other phase diagrams in order to show the details of the tricritical point and first order phase boundary.

However, the effective couplings are different for each phase. In the large negative J_K limit the AFM and AFM' phases have the following effective Ising couplings.

$$\begin{aligned} J_{\text{eff,AFM}} &= J_{x,y} - 2J_{K'} \\ J_{\text{eff,AFM}'} &= -J_{x,y} + 2J_{K'} \end{aligned} \quad (8)$$

Meanwhile, in the large positive J_K limit, for the FM and FM' phases

$$\begin{aligned} J_{\text{eff,FM}} &= J_{x,y} + 2J_{K'} \\ J_{\text{eff,FM}'} &= -J_{x,y} - 2J_{K'}. \end{aligned} \quad (9)$$

This behavior is similar to that of the Blume-Capel Model (BCM) which also approaches an Ising limit for large negative Δ which drives the density of vacancy sites

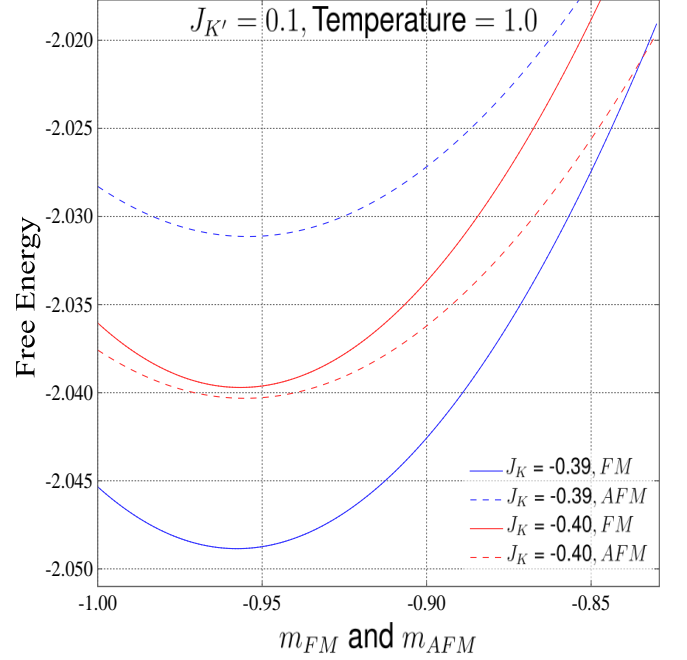


FIG. 7: (Color online) A plot of the FM and AFM free energies at $J_{K'} = 0.1$ and $T=1.0$ is shown. For $J_K = -0.39$ the minimum of the FM free energy (blue solid curve) is lower than the minimum of the AFM free energy (blue dashed curve) and therefore, the system is in the FM phase. For $J_K = -0.40$ the minimum of the FM free energy (red solid curve) is greater than the minimum of AFM free energy (red dashed curve) and therefore the system is in the AFM phase. If the global minima were to be at $m=0$, the system is in the PM phase where the total magnetization is 0. This is the analysis used to determine all of the first order phase boundaries in the mean field theory phase diagrams.

$M_i = 0$ to zero. However, our model does not approach the “vacant” lattice limit of the BCM at large positive Δ , because even though $S_i = -T_i$ in the AFM and AFM' phases, the individual nonzero S and T moments still couple down their respective chains. It is interesting, therefore, that, as we shall see, the tricritical points which are driven by vacancies in the BCM are still present in the CICM.

When $J_{K'} \neq 0$ the phase diagram loses its symmetry on changing the sign of J_K . As expected, for $J_{K'} = 0.1$ (Fig. 5), the AFM and FM phases meet at $J_K = -4J_{K'} = -0.4$. Also, for large, negative J_K , $T_c = 4(J_{x,y} - 2J_{K'}) = 3.2$ and for large, positive J_K , $T_c = 4(J_{x,y} + 2J_{K'}) = 4.8$; as $J_{K'} > 0$ gets larger, the FM phase gets larger and the AFM phase shrinks. The phase diagram is reflected about $J_K = 0$ for $J_{K'} = -0.1$ (not shown): the AFM region expands and the FM region shrinks.

Most importantly, the value of $J_{K'}$ determines whether or not there is a tricritical point. For $J_{K'} = 0.0$ and 0.1 , there is no tricritical point and all thermally driven phase transitions between an ordered phase and the disordered

phase are of second order. However, for $J_{K'} = 0.3$ (Fig. 6) there is a tricritical point. The thermally driven phase transition between the PM and the FM phase switches from second order to first order. The FM tricritical point emerges when $J_{K'} > \frac{1}{6}$, a result which follows from a detailed analysis of Eq. 5 and Eq. 7.

METROPOLIS MONTE CARLO

In order to achieve more accurate quantitative results, the Metropolis MC algorithm was implemented. We include moves which flip a single S spin, a single T spin, a row of S spins, a row of T spins, and an S and T spin simultaneously on a single site. Including this broad variety of cluster moves allows the system to reach thermal equilibrium more efficiently than in the case of just using single spin flips and is natural given the geometry. At each temperature of interest, the code ran for 5×10^5 MC sweeps (1 sweep = $2N$ steps) to thermalize and then another 5×10^5 MC sweeps while taking a measurement every ten sweeps.

In order to calculate the critical temperatures, the Binder fourth order cumulant,

$$U_L = 1 - \frac{\langle m^4 \rangle}{3 \langle m^2 \rangle^2} \quad (10)$$

where m is either m_{FM} , m_{AFM} , $m_{\text{FM}'}$, or $m_{\text{AFM}'}$ is calculated as a function of temperature for various lattice sizes, L . Curves for different lattice sizes have a common intersection point at the critical temperature (T_C), regardless of the order of the transition [24]. Additionally, the behavior of the Binder cumulant away from the crossing at T_C can be used to distinguish between first and second order phase transitions. For second order phase transitions, U_L approaches the value $U_L = \frac{2}{3}$ as the temperature approaches zero. For temperatures above the critical temperature, U_L approaches $U_L = 0$, all the while staying between these two values. For first order phase transitions, the Binder cumulant has the same limit values but, above the critical temperature, it develops a minimum that dips below 0 and which gets deeper for larger lattice sizes [24].

For $J_{K'}=0$, the MC phase diagram of Fig. 9 has the same qualitative features as the mean field phase diagram. In both cases there are two ordered phases at low temperatures, FM and AFM, and a PM phase at high temperatures. The AFM and FM phases meet, as expected, at $J_K = -4J_{K'} = 0$. Additionally, the MC phase diagram also contains the expected Ising regimes at large $|J_K|$, that is, $T_C \approx 2.269 J_{\text{eff}}$ [25]. For large positive J_K this leads to $T_C \approx 2.269 (J_{x,y} + 2J_{K'}) = 2.269$ and for large negative J_K , $T_C \approx 2.269 (J_{x,y} - 2J_{K'}) = 2.269$.

Similarly, for $J_{K'}=0.1$ (Fig. 10) the MC phase diagram qualitatively agrees with the mean field theory phase diagram. There is no tricritical point in either the mean

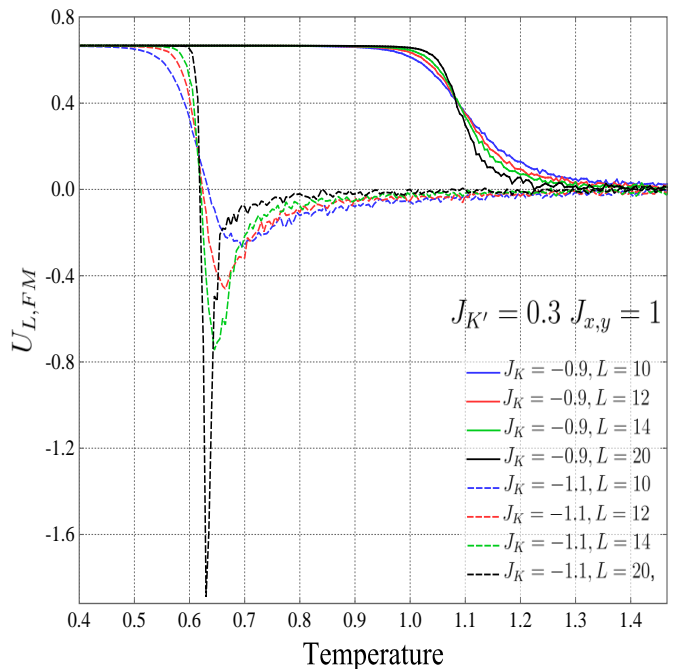


FIG. 8: (Color online) The Binder fourth order cumulants for various lattice sizes and for a second order phase transition (solid lines) at $J_K = -0.9$ and a first order phase transition (dashed lines) at $J_K = -1.1$. A minimum below $U_{L,FM}=0$, which gets deeper as the lattice size increases, is a signature of a first order phase transition. The curves intersect at a single critical temperature in both cases. U_L was used to determine all of the critical points in the MC phase diagrams.

field theory or MC phase diagrams and the FM and AFM phases meet at $J_K = -4J_{K'} = -0.4$ in both cases. For large positive J_K , we expect $T_C \approx 2.269 (J_{x,y} + 2J_{K'}) \approx 2.723$ and for large negative J_K , we expect $T_C \approx 2.269 (J_{x,y} - 2J_{K'}) \approx 1.815$, which agrees with the MC data.

Figure 11 shows MC results for $J_{K'}=0.3$. The FM and AFM phases meet at $J_K = -4J_{K'} = -1.2$, as in the MF phase diagram, and there is a FM tricritical point. One important qualitative difference between the MF and MC phase diagrams for $J_{K'}=0.3$ is that there is also an AFM tricritical point in the MC phase diagram. The MF phase diagram also has a small parameter window for $-1.2 \lesssim J_K \lesssim -1.1$ where raising T from the FM phase results in passage through an intermediate AFM phase before the disordered high temperature regime is reached. We have not reproduced this in the MC data.

Finally, in Figure 12 the phase diagram for $J_{K'}=1.0$ is shown. The FM and AFM' phases meet at $J_K = -2$, as expected from the ground state phase diagram. There is no tricritical point for this value of $J_{K'}$ which shows that there is some intermediate range between $J_{K'}=0.1$ and $J_{K'}=1.0$ where tricritical points are present.

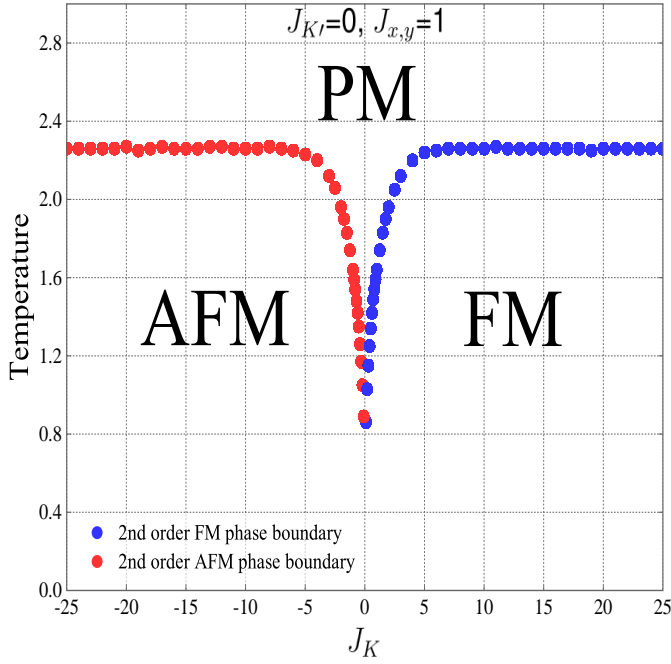


FIG. 9: (Color online) The MC-derived phase diagram for $J_{K'} = 0$ and $J_{x,y} = 1$ is shown. For $J_K > 0$, there is a second order phase boundary separating a low temperature FM phase from a high temperature PM phase. The critical temperature increases as J_K increases and saturates at $T_C \approx 2.269(J_{x,y} + 2J_{K'}) = 2.269$. For $J_K < 0$, there is a second order phase boundary separating a low temperature AFM phase from a high temperature PM phase. Similarly, the critical temperature increases as J_K decreases until it saturates at with $T_C \approx 2.269(J_{x,y} - 2J_{K'}) = 2.269$. This phase diagram is qualitatively similar to the MFT phase diagram with the same parameters, particularly in its lack of a tricritical point. As expected, the critical temperatures were overestimated in MFT.

WANG LANDAU SAMPLING

While the Metropolis MC algorithm is the most widely used method of numerically calculating the thermodynamic properties of classical spin models, there exist sophisticated alternatives. One is Wang-Landau sampling (WLS). In contrast to Metropolis MC, WLS numerically determines the density of states (DOS) and thus the partition function and, from that, all of the desired thermodynamic properties. The major advantage of WLS is that the DOS is independent of temperature so that only one simulation is needed to calculate thermodynamic quantities at any temperature. Additionally, the DOS can be used to calculate the unnormalized canonical distribution, $P(E)$,

$$P(E) \propto g(E) e^{-\beta E} \quad (11)$$

for various temperatures from one simulation. This distribution is another useful tool for distinguishing

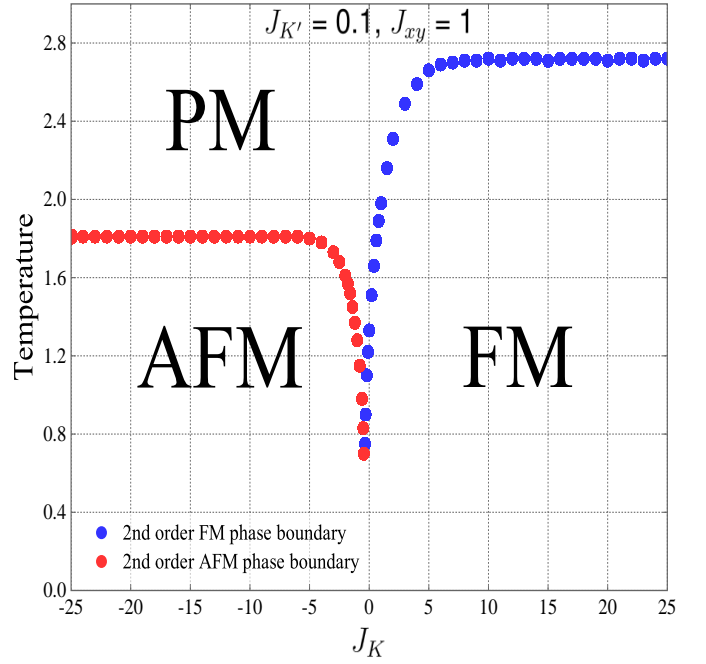


FIG. 10: (Color online) Same as Fig. 9 except $J_{K'} = 0.1$. The phase diagram is qualitatively similar to the result of MFT, particularly in its lack of a tricritical point.

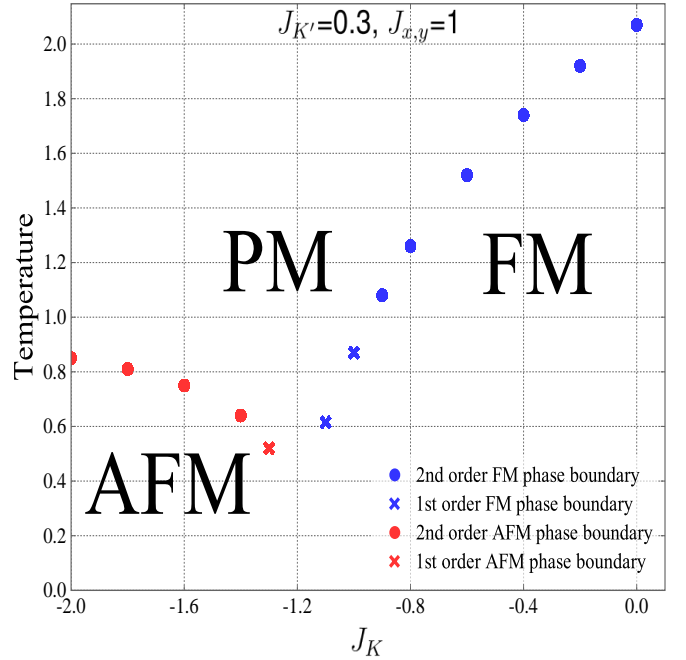


FIG. 11: (Color online) Same as Fig. 9 except $J_{K'} = 0.3$. The phase diagram is qualitatively similar to the result of MFT in most regards. However, MC finds that a tricritical point, which is present only on the FM side in MFT, is also present on the AFM phase boundary.

between first and second order phase transitions as it has

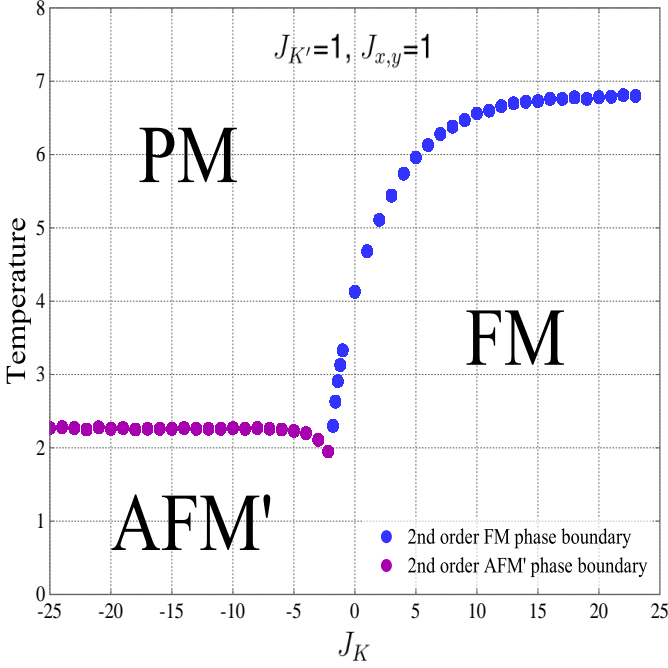


FIG. 12: (Color online) Same as Fig. 9 except $J_{K'} = 1.0$. As for $J_{K'} = 0.0$ and 0.1 , there is no tricritical point, which thus appear to be restricted to intermediate $J_{K'} \approx 0.3$.

distinct behavior in the two cases. For second order phase transitions, the canonical distribution is always a single peaked distribution which shifts its average value as the temperature changes. For first order phase transitions, the canonical distribution is similarly a single peaked distribution at temperatures well above and below the phase boundary. However, it develops a characteristic double peaked structure near the critical temperature due to phase coexistence. The peaks are of equal height precisely at the critical temperature [26].

This doubly peaked canonical distribution was found for our model as is shown in Fig.13, providing additional confirmation for the existence of the first order phase transition. Also, it provides a method of more precisely determining the first order critical temperature than the Binder cumulant method. For $J_K = -1.1$ and $J_{K'}=0.3$, the peaks were found to be of equal height at $T_c \approx 0.6173$. This procedure confirmed all three first order phase transition data points ($J_K=-1.3, -1.1, -1.0$) in the $J_{K'}=0.3$ MC phase diagram.

A clear and comprehensive detailing of the WLS algorithm can be found in the literature [21–23]. However, a few specific details of our simulations are worthy of mention. Every 10,000*2N spin flips, the histogram is checked for flatness. The flatness criterion used is that no individual energy is visited less than 80 percent of the average number of visits over all energies. When this criterion is achieved, the modification factor, f , which was initialized to $f=e$, is reduced ($f_{i+1} = \sqrt{f_i}$), the

histogram $H(E)$ is reset to zero and the process of spin flipping is continued. This algorithm continued until f was less than $e^{10^{-6}}$ at which time the density of states converged to our desired level of accuracy. The Wang Landau algorithm calculates the relative density of states and, therefore, the density of states was normalized as follows.

$$\ln(g_{\text{normalized}}(E_i)) = \ln(g_{\text{unnormalized}}(E_i)) - \ln(g_{\text{unnormalized}}(E_{GS})) + \ln(g_{\text{normalized}}(E_{GS})) \quad (12)$$

For our model, there are two ground states due to the spin inversion symmetry of the model.

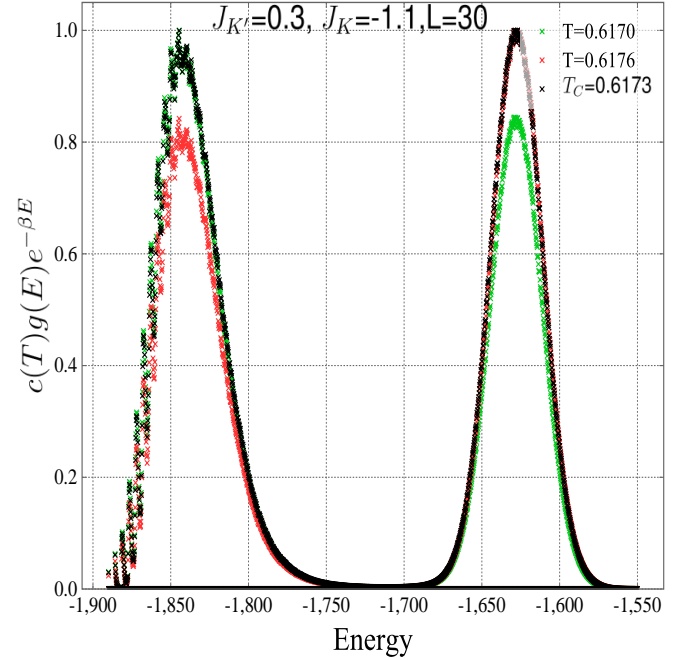


FIG. 13: (Color online) The canonical distributions from WLS for three temperatures above, at, and below the first order phase boundary at $J_K = -1.1$ and $T = 0.6173$ in the $J_{K'}=0.3$ phase diagram show the characteristic double peak behavior due to phase coexistence. At T_c (black data) the peaks are of equal height. The canonical distributions were normalized such that the peaks are equal to 1. This simulation was performed on a size $L=30$ lattice. For $L=10$ and $L=20$ lattices, the lower energy peak was smeared out and barely recognizable.

CRITICAL EXPONENTS

The CICM consists of Ising spins on one dimensional chains with interchain couplings that connect the system into a two-dimensional lattice and therefore, it is expected to belong to the two-dimensional Ising universality class where the magnetization exponent $\beta = \frac{1}{8}$. Precisely at a tricritical point the critical exponents

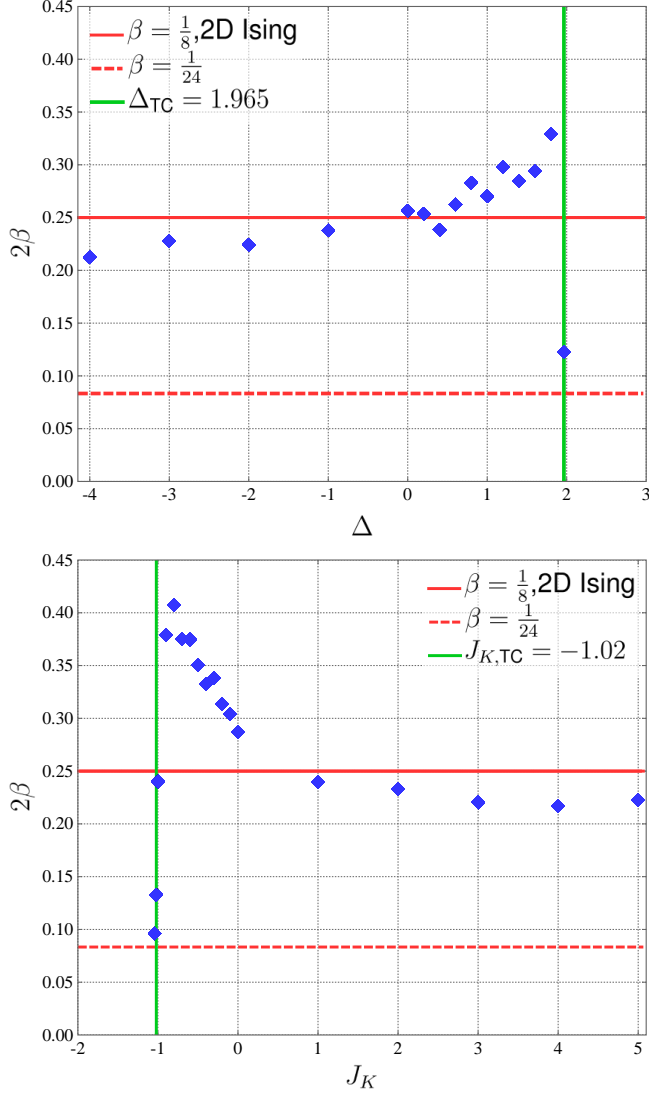


FIG. 14: The MC derived values of the critical exponent 2β for the BCM (top) and the CICM ($J_{K'} = 0.3$) (bottom) as a function of Δ and J_K , respectively, is shown for a $L=100$ lattice. In theory, $\beta = \frac{1}{8}$ (solid red line) away from the tricritical point and $\beta = \frac{1}{24}$ (dashed red line) precisely at the tricritical point. The tricritical point is given by the vertical green line. For both models, β is approximately the 2D Ising value of $\beta = \frac{1}{8}$ far from the tricritical point and then increases as the tricritical point is approached. At the tricritical point, the value drops close to the expected 2D tricritical Ising value of $\beta = \frac{1}{24}$. For the CICM, the left most point is at $J_K = -1.04$. Clearly, this point is closer to the known value of the tricritical exponent and therefore, this could be used as an alternative to the Binder cumulant in determining the position of the tricritical point.

take on different tricritical values. For the 2D tricritical Ising model, it is known that $\beta = \frac{1}{24}$ [27]. In Fig. 14, the value of 2β is plotted as a function of Δ and J_K for the BCM and the CICM, respectively. For both models, the exponents were determined by plotting the square

of the magnetization (for $L=100$ lattices) as a function of the reduced temperature (t) on a log-log scale and measuring the slope near $t=10^{-1}$. For both models, away from the tricritical point (which is located at the green line) the expected 2D Ising 2β (solid red line) is recovered to within the error bars due to the determination of T_C using the Binder cumulant ($\approx \pm 0.04$) plus some smaller finite lattice size errors. As the tricritical point is approached, an unusual non-monotonic behavior is observed, namely the critical exponents increase until, at the tricritical point, they suddenly drop to within the error bars of the expected tricritical value (dashed red line). For the CICM, the tricritical point was determined to be at $J_K = -1.02$ using the Binder cumulant. However, the left most data point shown in Fig. 14, at $J_K = -1.04$, gives a value for the tricritical exponent that is closer to its known value. Tuning the critical exponent to its known value may be an alternative method of determining the location of the tricritical point.

CONCLUSIONS

Using a combination of mean field theory, Metropolis Monte Carlo, and Wang Landau simulations, we have explored an Ising-like model on a lattice composed of a 1Dx1D collection of coupled chains. As is well known, 1D Ising chains with short range interactions do not exhibit finite temperature ordered phases. However, interchain couplings connect the chains into a 2D framework which shows multiple ordered phases at finite temperatures. The phase transitions between the ordered and disordered phases can be of first or second order as evidenced by the behavior of the Binder fourth order cumulants and the canonical distributions. The existence of tricritical points in the phase diagram depends on the value of $J_{K'}$. According to the MC simulations, for $J_{K'} = 0.1$ and 1.0 , there are no tricritical points but for intermediate $J_{K'} = 0.3$, there are tricritical points. The crossover of critical exponents from Ising to tricritical Ising values was observed to have an unusual non-monotonic behavior. As the tricritical point is approached, the order-parameter exponent β at first appears to rise substantially above the well-known Ising value of $\frac{1}{8}$ before falling sharply to a number close to the expected tri-critical value of $\frac{1}{24}$.

It would be interesting to see if the $\text{Nb}_{12}\text{O}_{29}$ materials can be tuned between first and second order transitions by varying pressure, doping or other parameters, thus giving rise to novel realizations of tricritical systems. However, our work suggests that some caution is needed, in that tricritical exponent values may be masked by rapid non-monotonic variations making it difficult to observe asymptotic exponent values in experiments.

In some materials which exhibit this 1Dx1D geometry, the quantum mechanical nature of the degrees of freedom

may be crucial to the observed phenomena. For example, in the optical lattice case, the focus is on the occurrence of Bose-Einstein condensation at finite momentum, and in a pattern of orbitals which alternates as $p_x \pm ip_y$ on the two sublattices. Our work shows that even at the classical level, these crossed-chains systems exhibit complex phase-transitions and crossovers. Future work should address the additional non-trivial physics which arises when the phase transitions are driven to $T = 0$, giving rise to exotic quantum phase transitions.

TC and RTS were supported by Department of Energy grant de-sc0014671. The work of RRPS is supported by the US National Science Foundation grant number DMR-1306048.

-
- [1] “Equilibrium Statistical Mechanics of Lattice Models,” D. Lavis, Springer, Netherlands (2015).
 - [2] “Critical properties of site- and bond-diluted Ising ferromagnets,” J.M. Yeomans, R.B. Stinchcombe, Journal of Physics C: Solid State Physics 12, 2 (1979).
 - [3] “Critical Phenomena on Fractal Lattices,” Y. Gefen, B. Mandelbrot, and A. Aharony, Phys. Rev. Lett. Volume 45, Number 11, (1980).
 - [4] “Ising Model with a Long-Range Interaction in the Presence of Residual Short-Range Interactions,” George A. Baker, Jr., Phys. Rev. 130, 1406 (1963).
 - [5] “Ising Chain with Competing Interactions,” John F. Nagle, Phys. Rev. A2, 2124 (1970).
 - [6] “Critical Behavior of Ising Models with Random Long-Range Interactions,” R.T. Scalettar, Physica A170, 282 (1991).
 - [7] “Exact solution of Ising model on a small-world network,” J. Viana Lopes, Yu. G. Pogorelov, and J. M. B. Lopes dos Santos, Phys. Rev. E70, 026112 (2004).
 - [8] “Small-world phenomena in physics: the Ising model,” M. Gitterman, J. Phys. A: Math. Gen. 33, 8373 (2000).
 - [9] “Organometallic-like localization of 4d-derived spins in an inorganic conducting niobium suboxide,” K.-W. Lee and W. E. Pickett, Phys. Rev. B91, 195152 (2015).
 - [10] “Antiferromagnetism and metallic conductivity in $\text{Nb}_{12}\text{O}_{29}$,” R.J. Cava, B. Batlogg, J.J. Krajewski, P. Gammel, H.F. Poulsen, W.F. Peck, Jr., and L.W. Rupp, Jr., Nature 350, 598 (1991).
 - [11] “Nanometer structural columns and frustration of magnetic ordering in $\text{Nb}_{12}\text{O}_{29}$,” E.N. Andersen, T. Klimczuk, V.L. Miller, H.W. Zandbergen, and R.J. Cava, Phys. Rev. B72, 033413 (2005).
 - [12] “Optical Lattices,” M. Greiner and S. Fölling, Nature 453, 736 (2008).
 - [13] “Multiflavor bosonic Hubbard models in the first excited Bloch band of an optical lattice,” A. Isacsson and S.M. Girvin, Phys. Rev. A 72, 053604 (2005).
 - [14] “Unconventional Bose-Einstein Condensation Beyond The ”No-Node” Theorem,” C. Wu, Mod. Phys. Lett. B 23, 1 (2009).
 - [15] “Atomic matter of nonzero-momentum Bose-Einstein condensation and orbital current order,” W. V. Liu, and C. Wu, Phys. Rev. A 74, 013607 (2006).
 - [16] “Exotic phases of p -band bosons in interaction,” F. Hébert, Zi Cai, V.G. Rousseau, Congjun Wu, R.T. Scalettar, and G.G. Batrouni, Phys. Rev. B87, 224505 (2013).
 - [17] “Exact Results for Itinerant Ferromagnetism in Multiorbital Systems on Square and Cubic Lattices,” Yi Li, Elliott H. Lieb, and Congjun Wu, Phys. Rev. Lett. 112, 217201 (2014).
 - [18] “Theory of the First-Order Magnetic Phase Change in UO_2 ,” M. Blume, Phys. Rev. 141, 517 (1966).
 - [19] “On the possibility of first-order phase transitions in Ising systems of triplet ions with zero-field splitting,” H.W. Capel, Physica 32, 966 (1966).
 - [20] “A Guide to Monte Carlo Simulations in Statistical Physics,” D.P. Landau and K. Binder, Cambridge University Press (2000).
 - [21] “Efficient, Multiple-Range Random Walk Algorithm to Calculate the Density of States,” F. Wang and D.P. Landau, Phys. Rev. Lett. 86, 2050 (2001).
 - [22] “Determining the density of states for classical statistical models: A random walk algorithm to produce a flat histogram,” F. Wang and D.P. Landau, Phys. Rev. E64, 056101 (2001).
 - [23] “Determining the density of states for classical statistical models by a flat-histogram random walk,” D.P. Landau and F. Wang, Comput. Phys. Commun. 147, 674 (2002).
 - [24] “Finite size effects at thermally-driven first order phase transitions: A phenomenological theory of the order parameter distribution,” K. Vollmayr, J.D. Reger, M. Scheucher, and K. Binder, Z. Phys. B 91, 113-125 (1993).
 - [25] “Crystal Statistics. I. A Two-Dimensional Model with an Order-Disorder Transition,” Lars Onsager, Phys. Rev. 65, 117 (1944).
 - [26] “Finite-size effects at temperature-driven first-order transitions,” M. S. S. Challa, D. P. Landau, and K. Binder, Phys. Rev. B 34, 18411852, (1986).
 - [27] “Exact Critical Point and Critical Exponents of $\text{O}(n)$ Models in Two Dimensions,” Bernard Nienhuis, Phys. Rev. Lett. 49, 1062, (1982).